Available online at www.sciencedirect.com
ScienceDirect
Simulation Modelling Practice and Theory 15 (2007) 764–785
SIMULATION MODELLING PRACTICE AND THEORY
www.elsevier.com/locate/simpat

Modelling and simulation of a wireless microsensor data acquisition system using PCM techniques

Khalil Arshak *, Essa Jafer, Declan McDonagh

Electronic and Computer Engineering, University of Limerick, Plassey Technological Park, 02098 Limerick, Ireland

Received 18 May 2005; received in revised form 14 March 2007; accepted 10 April 2007
Available online 27 April 2007

Abstract

This paper presents a review of developed simulated models for a wireless data acquisition system. The system reads analogue information provided by two sensors used for medical purposes. The real data have been recorded by two, pH and pressure sensors used in diagnosing conditions of the esophagus that are employed to examine the system performance. The created model contains four main simulated units using SIMULINK. The first unit contains the output signal, which is encoded to digital signal based on adapting one of the pulse coding modulation (PCM) algorithms. The second unit simulates the processor function that is responsible for framing, mixing and compressing the incoming bit streams from both sensors. The third unit, where the digital data are modulated and sent through different noisy channels, represents an efficient FSK transmitter/receiver model. At the receiver end, the signal is demodulated and processed inversely to extract the original analogue signal read by the two sensors.

In this work, the performance of the systems using different PCM methods will be studied comparatively in order to control the transmission and reduce the amount of data frames sent. This will lead to a significant reduction in power consumption. In addition, the performance of the RF unit through additive White Gaussian noise (AWGN) channel was examined by estimating the average bit error rate (BER) for different carrier frequencies. The effect of the multipath fading, inband/outband interference, and adjacent channel power ratio (ACPR) has also been investigated during system assessment.

Keywords: SIMULINK; Modelling; Data acquisition; Pulse coding modulation; Frequency shift keying; Short-range wireless

1. Introduction

Recent advances in integrated sensors have made a realization of smart microsystems combining a large mixture of micro-sensors and signal processing circuitries. This will have a significant impact on a variety of applications such as health care, consumer electronics, environmental monitoring and medical diagnosis [1,2].

* Corresponding author. Tel.: +353 61202267; fax: +353 61338176.
E-mail address: khalil.arshak@ul.ie (K. Arshak).

1569-190X/$ - see front matter
doi:10.1016/j.simpat.2007.04.006

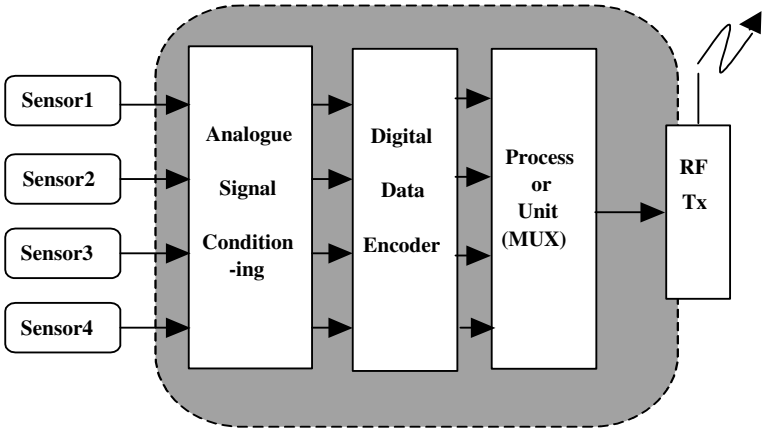

Fig. 1. Block diagram of telemetry multi-sensors system.

Such systems are required to have many attributes, such as low cost, robustness and real-time data processing. The need for wireless communication is increased by the high cost of wiring and the growing demand for distributed and remote sensing, data acquisition, and control. Sensor manufacturers are integrating RF systems in the same enclosure as their sensing devices. Wireless communication is a viable and cost-effective method of transmitting data over long distances, through electrically noisy environments. A number of telemetry-based medical systems have been developed for different implanted applications [3–5].

A general block diagram of a telemetry data acquisition system is depicted in Fig. 1. It consists of analog stage, where a signal read by the sensors is recorded, digitally encoded where the signal will be converted to a bit stream, processor unit and RF unit that combines both transmitter and receiver circuitry.

SIMULINK is windows based program for simulating dynamic systems. A block structured approach for modelling is employed. Any inter-block connections that may be required are made before the system is ready to be simulated using one of a range of numerical integration algorithms. One attractive feature is the ability to group associated blocks together to form a single block. This block has all the functionality of the original blocks but is represented on screen in a more simple form.

In this paper, a data acquisition system has been modelled, simulated and tested. Pressure and pH sensors signals are employed for system performance assessment as they have a significant role in biomedical monitoring and diagnosing [6]. The novelty in this work is based on using SIMULINK to build a very realistic complete model for a medical telemetry system that is incorporating some real signals to get credible simulation results. Three PCM algorithms have been introduced in the system to achieve high data compression; which will be presented in the next sections.

2. System specifications

Fig. 2 shows the main task and functions that should be implemented by the proposed system. In the first stage, two different analog signals obtained from a real data [7] are introduced and encoded into digital signal. The sources of the two signals are a pH and pressure sensors that have been used to record both acidity and electrical activity of the esophagus.

The obtained recording pressure data of the esophagus electrical activity is a combination of noise and periodical signals. The pressure signal has an amplitude level change from 0 to 50 mmHg with a mean value of 18.34 mmHg as shown in Fig. 3. The mean power of the corresponding peak frequency was found to be 13.46 ± 1.36 dB. The noisy part of the signal represents the respiratory artifact which is very annoying problem since its frequency is very close to that of the real pressure signal. Pressure waves in the esophagus have a sinusoidal form, so the data can be encoded without loss of useful information as a train of pulses. Sampling

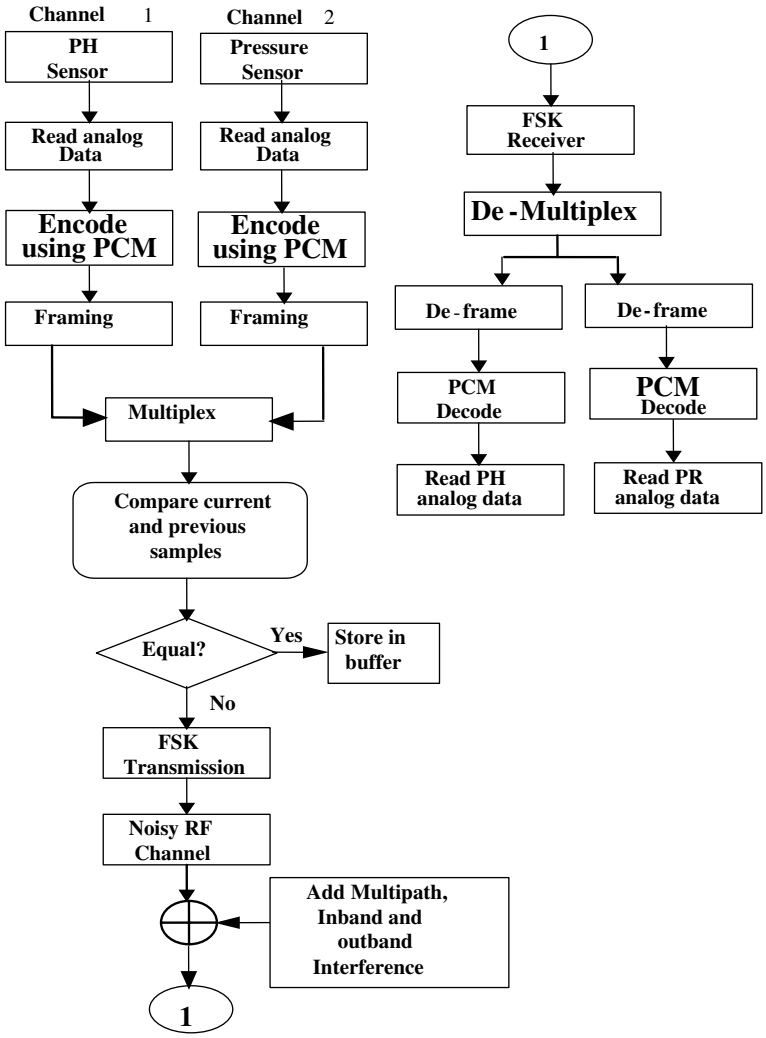

Fig. 2. Description flowchart of the proposed wireless multi-channel system.

period of 8 ms was chosen to digitize efficiently the two analog coming signals. It has been noted that the rate of change of the two analog data is quite different, such that pressure signal is rapidly changing in a random way, while the pH taking a relatively stable values over a certain periods.

The system functions can be divided into four main stages. The output of the first stage is a digital encoded bit stream using a PCM algorithm, which will be described in the next section. The two binary data streams coming from the two channels are processed by the controller unit, which represents the second stage. The data coming from each channel is framed, multiplexed and compressed at this stage before it is sent to RF unit. At this stage, the serial binary stream will be modulated using FSK and sent through a noisy RF channel to the receiver. The data are then demodulated at the receiver side and inversely processed to recover the two analog signals. The PCM methods used in this system are the uniform quantization, non-uniform quantization, differential pulse code modulation and adaptive pulse code modulation.

The performance of the simulated system will be assessed in two stages. At first stage, the effect of data compression implemented by the controller unit and tested with different PCM methods. Then the RF channel performance for a certain range of frequencies is investigated for different conditions.

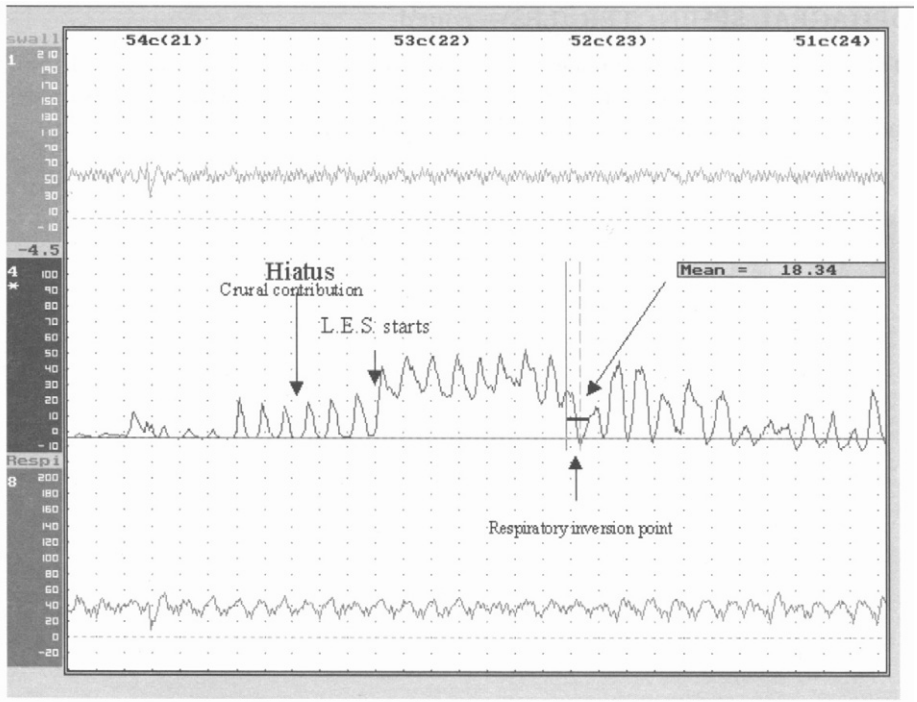

Fig. 3. Recorded pressure changes at the lower part of the esophagus.

3. Pulse code modulation algorithms (PCM)

PCM is the most obvious method developed for digital coding of waveforms and it is often used for speech signals, which have a non-stationary nature. Essentially it refers to a process of quantizing the samples of discrete-time signal, so that both time and amplitude are represented in a discrete form. Three different PCM methods have been adapted in the proposed system, these are given in [8,9].

3.1. Uniform pulse code modulation (UPCM)

It is a digital representation of an analog signal where the magnitude of the signal is sampled regularly at uniform intervals of duration. Every sample is quantized to a series of symbols in a digital code, which is usually a binary code. A uniform quantizer with an even number of outputs values is employed in this method. For a uniformly distributed input variable x with standard deviation σ and zero mean, the probability density function (PDF) is:

$$f_x(x) = \begin{cases} \frac{1}{2\sqrt{3}\sigma}, & |x| \leqslant \sqrt{3}\sigma, \\ 0, & \text{otherwise.} \end{cases} \tag{1}$$

3.2. Nonuniform pulse code modulation (NPCM)

For a non-uniform quantizer, the input is first transformed with a memoryless monotonic nonlinearity to produce an output $f(x)$.Then it is uniformly quantized with the quantized values transformed by the inverse nonlinearity. One of the two main logarithmic functions that have become widely used as design guidelines for non-uniform quantization is the μ-law function, which is given by:

$$f(x) = A\frac{\ln(1+\mu|x|/A)}{\ln(1+\mu)}\operatorname{sgn}(x), \quad |x| \leqslant A, \tag{2}$$

where A is the peak-input magnitude and μ is a constant that controls the degree of compression. The prevailing μ value used in practice is 255.

3.3. Differential pulse coding modulation (DPCM)

DPCM is based on the notion of quantizing the prediction-error signal. In many signal sources, samples are correlated with their neighbors, so the current sample can be easily predicted from the past history by forming the prediction-error signal. By quantizing the prediction error, a higher signal-to-noise (SNR) ratio can be achieved for a given resolution. This method is presented in Fig. 4, where the prediction error $e[n]$, obtained by subtracting the input $x[n]$ from the prediction $x_p[n]$, is quantized. The indices at the output of the quantizer's encoder represent the DPCM bit stream. The DPCM decoder works in a similar fashion to the encoder in order to obtain the quantized samples from the indices [8].

4. SIMULINK®PCM encoder model

The basic units of this model are shown in Fig. 5 [10]. Basically the two stored signals (pH and pressure) will be sampled first and then converted to a digital data using one of the three PCM algorithms (referred as subsystem in the figure). Then a binary (bipolar) signal is generated from as a bit stream using serial to parallel special function. The two output bit streams are saved into files before using them in the next system stages.

5. Simulation of the controller unit

This unit has been modeled so that the following tasks can be achieved:

1. Framing the input coded bit streams coming from the PCM stage.
2. Control the operation of the RF transmitter/receiver by compress the amount of serial bits to be transmitted.
3. Multiplex the pH and pressure frames into a single frame with a start and end flag as shown in Fig. 6.
4. Outputs a serial bit stream to the RF transmitter at a bit rate or 2.5 kbps.

A data compression mechanism based on sending only the unrepeated frames has been adapted. This will lead to reduce the amount of data bits to be transmitted and minimize the overall power consumption of the system. According to this, each frame may have one or more of the pH and pressure 8 bits fields to be filled with zeros.

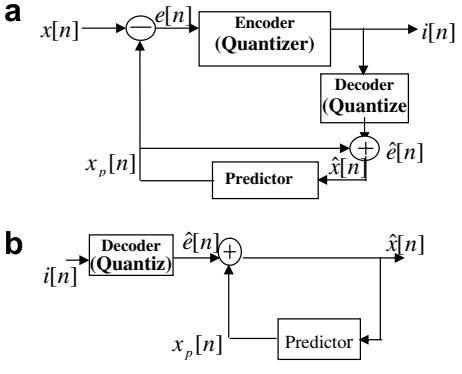

Fig. 4. Differential pulse coding (DPCM): (a) encoder, (b) decoder.

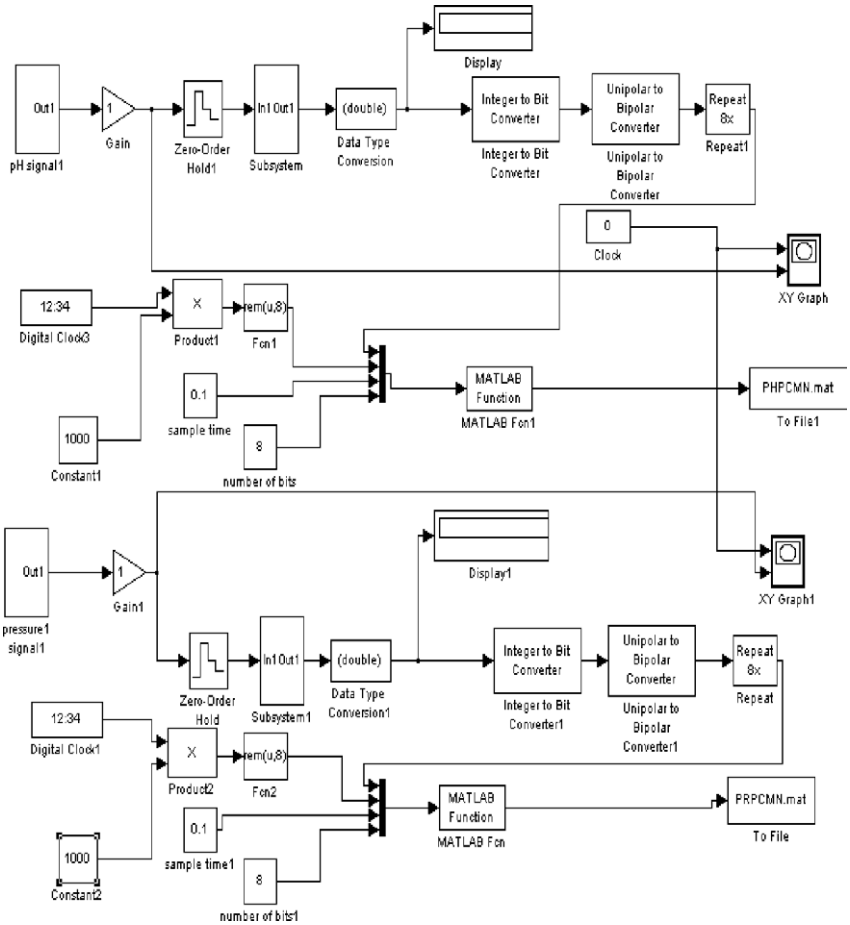

Fig. 5. Block diagram of the PCM encoding unit.

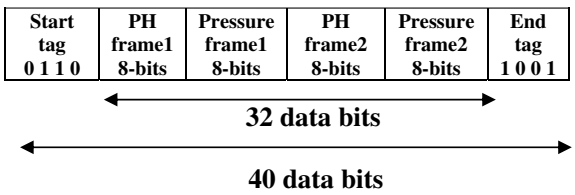

Fig. 6. Output data frame of the processor unit.

Fig. 7 shows a capture view of the output bit stream from the simulated processor unit. The time pause, where there is no transmission, can be noticed with different durations

6. Short-range wireless communication (SRWC)

Short-range wireless is a complementary class of emerging technologies meant primarily for indoor use over very short distances. SRWC links will offer peak speeds of tens or even hundreds of megabits per second at very low cost and with very low power to many closely spaced users. Over the past several years, driven by data applications, very short-range systems have emerged with maximum ranges of 10–100 m. In general four trends have been driving the growth of the short-range wireless communication:

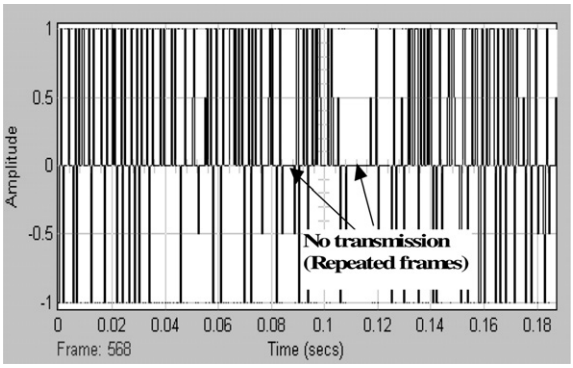

Fig. 7. Sample of output data after compression.

1. Increasing the demand for wireless data capability in portable devices at higher bandwidth and at lower cost and power consumption.
2. Growth of indoor wireless communication with different transmission frequencies.
3. Shrinking the semiconductor cost and power consumption for signal processing.

Wireless transmitters and receivers can be conceptually separated into baseband and RF sections [11]. Baseband is the range of frequencies over which transmitters take their input and receivers produce their output. The RF section of the transmitter is responsible for converting the processed baseband signal up to the assigned channel and injecting the signal into the medium. One of the main goals of the transmitter is to transmit a specified amount of power while consuming a little power as possible. For the receiver, the design requirements must faithfully recover small signals and reject interference outside the desired channel.

RF systems are constructed primarily by using four basic building blocks; there are amplifiers, filters, mixers, and oscillators [12].

Two main RF receiver architectures were considered in this work. First is the *Heterodyne* receiver which converts the input to intermediate frequency (IF), perform band-pass filtering and amplification, and translate the spectrum to a lower frequency again. Direct conversion is the second type where the channel of interest is translated to zero frequency as shown in Fig. 8. Direct-conversion architecture proved to have two advantages over the *Heterodyne* counterpart [12]. First there will be no need for an image rejection filter, since the intermediate frequency will be zero. Second, the IF filter and the subsequent down-conversion stages are replaced with low-pass filters and baseband amplifiers that are amenable to monolithic integration [13].

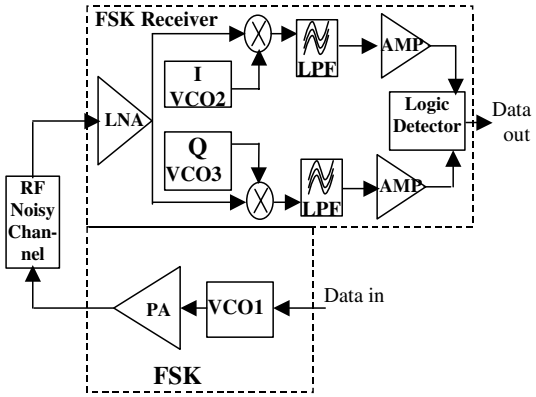

Fig. 8. Illustrates the architecture of the simulated direct-conversion FSK transmitter/receiver.

6.1. Frequency shift keying (FSK) transmitted signal

Generally the two generated FSK tones can be described using the following equation:

$$X(t) = A(t)\cos((w_s \pm w_c)t), \tag{3}$$

where a is the signal amplitude, w_s and w_c are the carrier and frequency shifts, respectively. The two signals are used to transmit equally likely bits over a noisy channel. The FSK signal amplitude (a) can be expressed in terms of bit energy E_b and bit time interval T_b as follows:

$$a = \sqrt{\frac{2E_b}{T_b}}. \tag{4}$$

6.2. Multipath fading channel

The multipath and motion induced fading are the two of the most severe performance limiting phenomena that occur in wireless radio channels. To illustrate the basic approach to modeling fading channels, the channel output from N-path case can be described by the following equation [14]:

$$y(t) = \sum_{n=1}^{N} a_n(t)x(t - \tau_n(t)) \tag{5}$$

where $y(t)$ and $x(t)$ are multipath fading and transmission path signals, $a_n(t)$ and $\tau_n(t)$ represent attenuation and propagation delay associated with nth multipath component. Substituting (3) into (5) gives:

$$y(t) = a_n(t)A(t - \tau_n(t))\cos(w_s \pm w_c)(t - \tau_n(t)). \tag{6}$$

The above equation can be written as

$$y(t) = \sum_{n=1}^{N} a_n(t)A(t - \tau_n(t))\mathrm{RE}\{\exp[\mathrm{j}(w_s \pm w_c)t]\exp[-\mathrm{j}(w_s \pm w_c)\tau_n(t)]\}. \tag{7}$$

Since $a_n(t)$ and $A(t)$ are both real, then:

$$y(t) = \mathrm{RE}\{a_n(t)A(t - \tau_n(t))\exp[\mathrm{j}(w_s \pm w_c)t]\exp[-\mathrm{j}(w_s \pm w_c)\tau_n(t)]\}. \tag{8}$$

From the above equation, the complex path attenuation $\tilde{a}_n$ can be defined as:

$$\tilde{a}_n(t) = a_n(t)\exp[-\mathrm{j}(w_s \pm w_c)\tau_n(t)]. \tag{9}$$

Therefore, the above equation can be expressed in term of the complex signal envelop and phase as follows:

$$y(t) = \mathrm{RE}\left\{\sum_{n=1}^{N} \tilde{a}_n(t)A(t - \tau_n(t))\exp[-\mathrm{j}(w_s \pm w_c)]\right\}. \tag{10}$$

The envelop of the combined signal $\tilde{y}(t)$ at the receive input is:

$$\tilde{y}(t) = \sum_{n=1}^{N} \tilde{a}_n(t)A(t - \tau_n(t)). \tag{11}$$

7. FSK transmitter/receiver SIMULINK implementation

In this section, a detailed description of the simulated FSK transceiver model is given as follows.

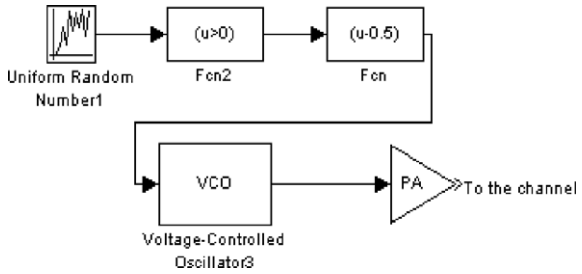

Fig. 9. Modelling FSK transmitter.

7.1. FSK transmitter model

A simple FSK modulator is simulated and implemented using SIMULINK® as shown in Fig. 9. In this model, a uniform random number generator is employed to output a random bit stream of 0 and 1's with a specific data rate. The input voltage of the voltage controlled oscillator (VCO) is shifted either to ± 0.5 instead of 0 or 1. This is implemented in order to get an equal frequency shift for both tones by multiplying this input value by the sensitivity of the VCO.

The power amplifier (PA) is modeled to be a nonlinear unit since it exhibits a higher efficiency of 60% for some of the power efficient modulation techniques as the FSK [15]. This can be explained, as the FSK waveforms have no abrupt phase change and exhibit a constant envelope. Therefore the FSK signals can be amplified by means of nonlinear PA's with no spectral regrowth.

7.2. FSK receiver model

A direct-conversion *homodyne* receiver is modeled as shown in Fig. 10. The low-noise amplifier (LNA) represents the first gain stage in the receiver path and its noise figure is added directly to that of the system. A small signal nonlinearity, compression, saturation, slew rate limiting, and two types of noise (white and flicker) are modeled within the (LNA) unit as shown in Fig. 11.

The output RF signal from the (LNA) unit is mixed with two quadrature oscillators that generate a frequency equal to the input carrier frequency. Two low-pass filters (LPFs) with relatively sharp cutoff characteristics are used for both channels selections. A butterworth analog filter with order 3 was selected to implement these two units.

7.3. Symbol (logic) detector

This block has a crucial effect on the system overall performance and its design needs to be fully understood. The main function of the unit is to recover properly the bit symbols of the input signal using a logic system. The details of this unit in SIMULINK® are shown in Fig. 12.

As shown above, a combinational logic units process the incoming signals from the two-quadrature channels. The output bit value is extracted at the final stage by S-R flip-flop.

8. Modeling channel propagation effects

One of the challenges in channel modeling is the translation of the detailed physical propagation into a form that is suitable for simulation.

The SIMULINK® is a powerful tool that has huge advantages in being able to build realistic mathematical models. In Fig. 13, a propagation channel model for a single path FSK signal with two effects, adding additive White Gaussian noise (AWGN) and short distance (0.5 m) path loss, is presented.

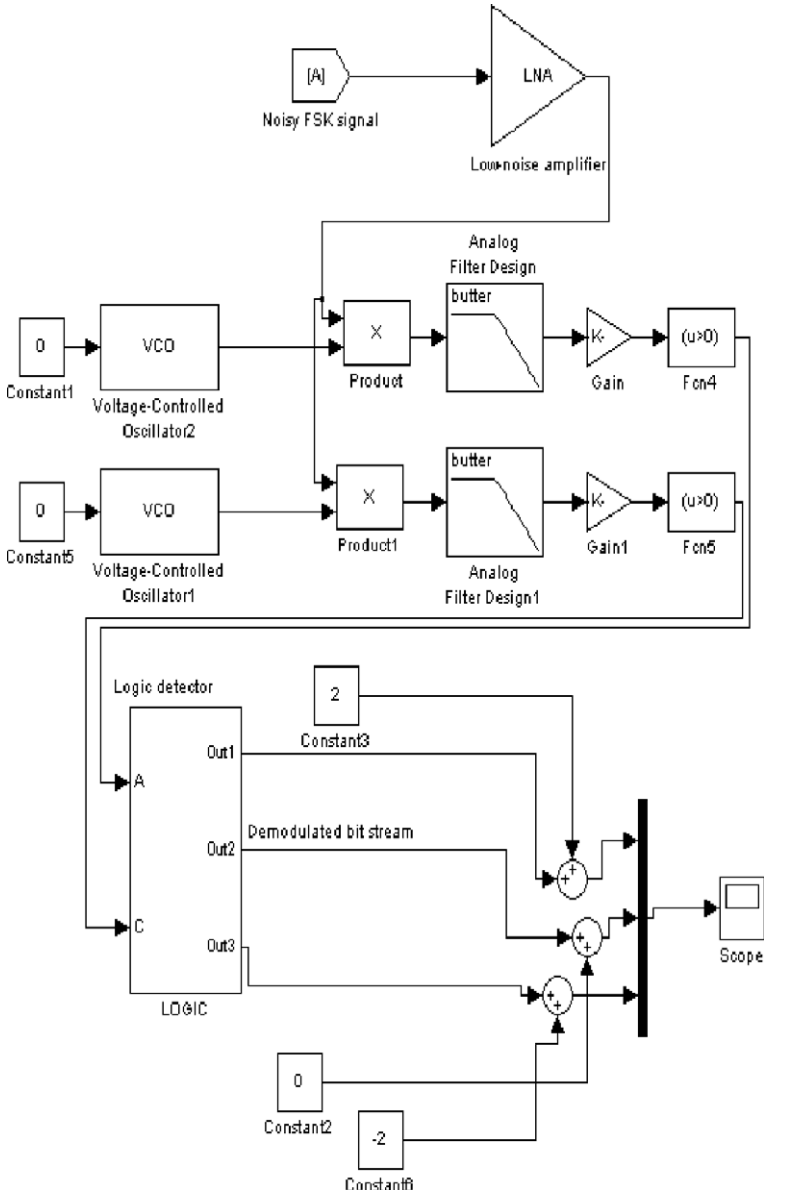

Fig. 10. Modelling FSK direct-conversion receiver.

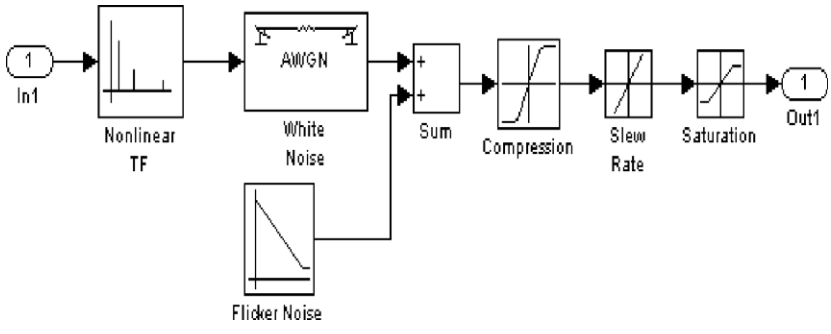

Fig. 11. Modelling a nonlinear LNA unit.

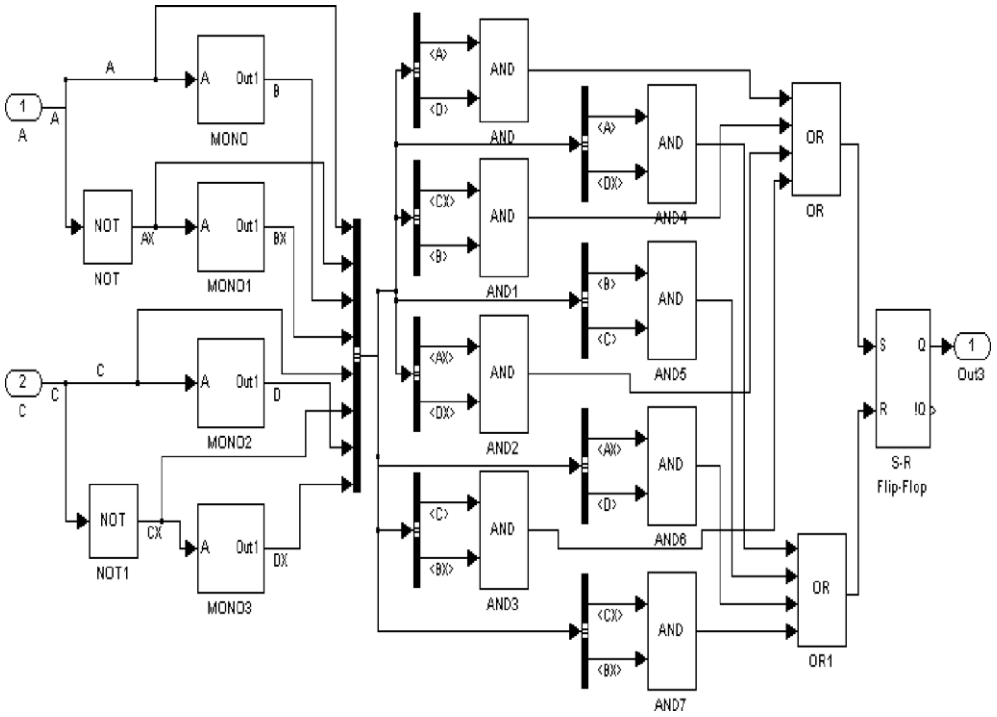

Fig. 12. Modelling symbol logic detector.

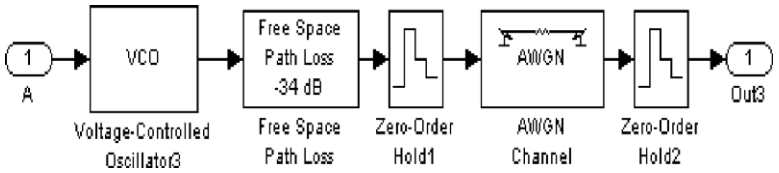

Fig. 13. Modelling channel with White noise and path loss.

8.1. Rayleigh multi-path fading model

In case of indoor short-range wireless communications, propagation may be classified as line of sight (LOS) where the transmitter and receiver are visible to one another or abstructed (OBS), where objects in the channel block have a visible propagation path [16]. Rayleigh distribution is commonly used to describe time varying nature of the received envelope of a flat fading signal. Fig. 14 shows a SIMULINK® implementation of a three-rays Rayleigh fading model.

Rayleigh generator unit is based on the rule that summing two quadrature Gaussian noise signals obeys a Rayleigh distribution. The probability distribution function (pdf) of Rayleigh distribution is given by the following equation:

$$p(r) = \begin{Bmatrix} \frac{r}{\sigma^2}\exp\left(-\frac{r^2}{2\sigma^2}\right) & 0 \leqslant r \leqslant \infty \\ 0 & r \prec 0 \end{Bmatrix} \tag{12}$$

where σ^2 is the time average- power of the received signal before detection. The mean value r_{mean} of the Rayleigh distribution is given by:

$$r_{\text{mean}} = E(r) = \int_0^\infty rp(r)\,\mathrm{d}r = 1.2533\sigma. \tag{13}$$

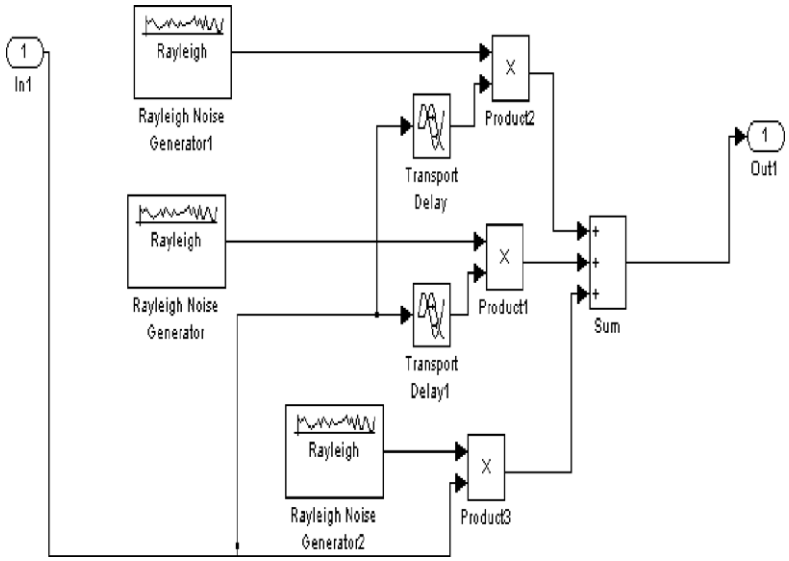

Fig. 14. Modelling of multipath Rayleigh fading channel.

The variance of Rayleigh distribution is given by σ_r^2, which represents the ac power in signal envelop as follows:

$$\sigma_r^2 = E[r^2] - E^2[r] = \int_0^\infty r^2 p(r)\,\mathrm{d}r - \frac{\sigma^2\pi}{2} = 0.4292\sigma^2. \tag{14}$$

The median value (r_{median}) is found by solving:

$$\frac{1}{2} = \int_0^{r_{\text{median}}} p(r)\,\mathrm{d}r \Rightarrow r_{\text{median}} = 1.177\sigma. \tag{15}$$

Thus the mean and the median should differ only by 0.55 dB in Rayleigh fading signal.

The time delay units represent the multipath delay time spreads and they typically take values up to 100 ns for outdoor propagation and between 30 and 60 ns for indoor propagation [16].

8.2. Inband and outband interference model

Interference is a major limiting factor in the performance of wireless RF systems. Sources of interferences include another transmitter devise operating either in the same frequency or neighboring frequency bands. The two major types of system-generated interference are co-channel (in band) and adjacent (outband) channel interference. Inband channel interference is defined as undesired signals with frequency components that fall within the receiver's RF passband. On other hand, outband channel interference is defined as signals with frequency components that are significantly removed from the receiver's RF passband.

In SIMULINK®, a simple model for system interference can be constructed by combining the output signals from a number of different FSK transmitters as shown in Fig. 15.

The adjacent power interference (ACI) refers to signals with frequency components, which fall near the channel passband, its effect will be investigated in the following section.

9. Testing FSK system performance

9.1. FSK transceiver performance

The FSK transmitter/receiver model was simulated and tested as its performance has a direct influence on the overall system operation. Samples of unipolar modulated and demodulated signals at carrier frequency of 100 MHz are shown in Fig. 16.

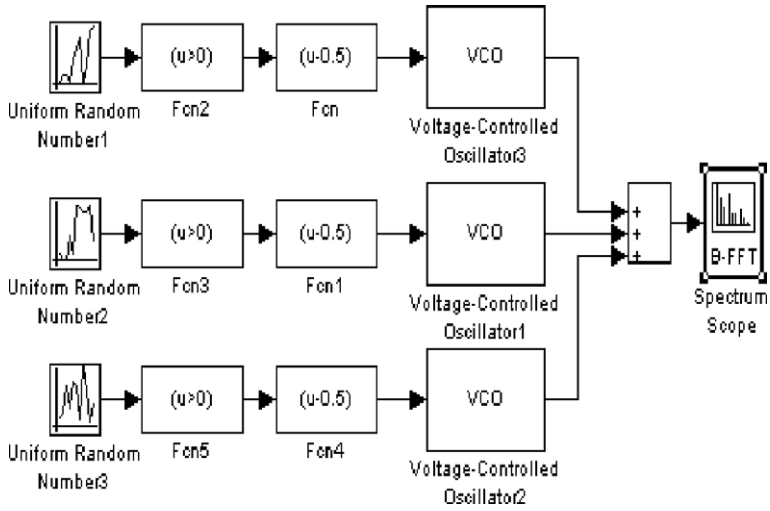

Fig. 15. Modelling the system interference.

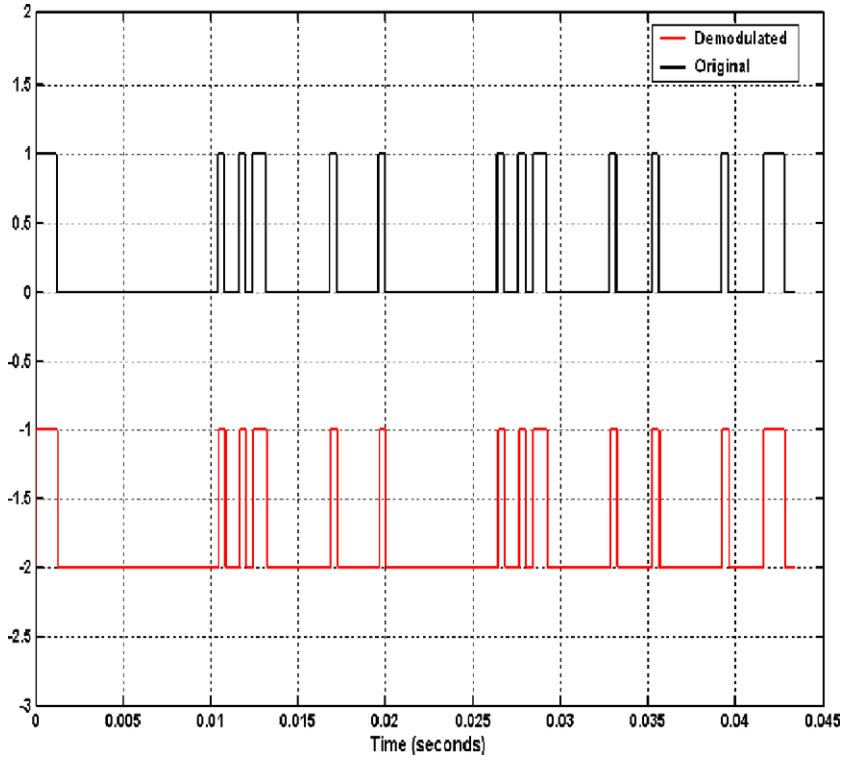

Fig. 16. Original and demodulated using FSK receiver with a carrier frequency of 100 MHz.

Fig. 17 shows the constellation diagram (quadrature complex signal projection) of noisy FSK signal with signal-to-noise ratio (SNR) 15 dB.

9.2. Estimation bit error rate (BER) of the system

Initially, the bit error rate (BER) parameter is used to assess the performance of the transceiver for three different FSK carrier frequencies (20, 50, 100 MHz) with a bit rate of 20 kbps as shown in Fig. 18. The BER is

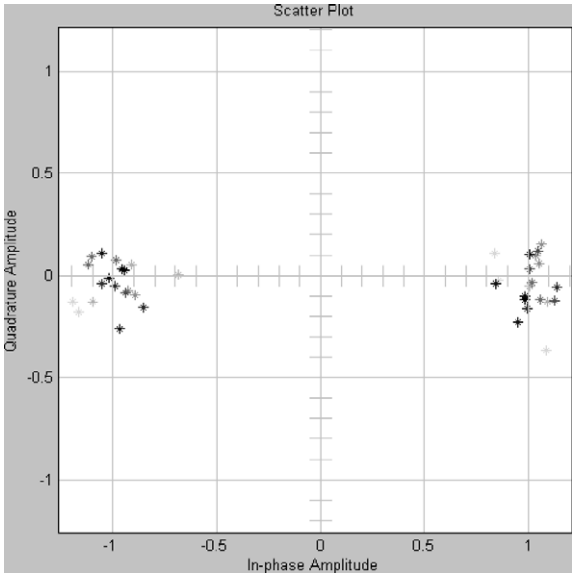

Fig. 17. Constellation diagram of noisy FSK signal with SNR = 15 dB.

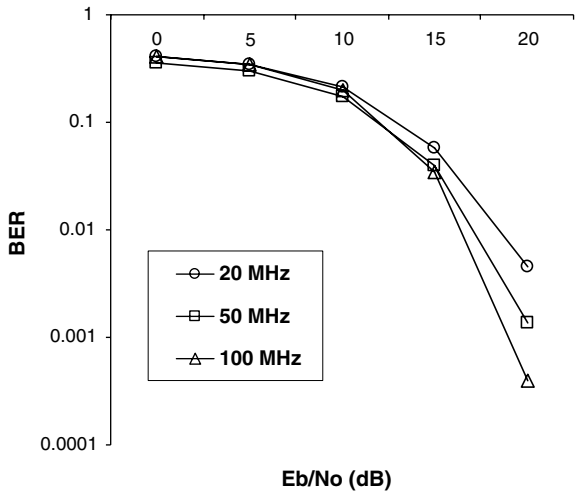

Fig. 18. BER performance against bit energy to noise power ratio (E_b/N_o) of the RF channel for three different FSK carrier frequencies.

improved when the SNR and the transmission carrier frequency have been increased. It is worth to mention that the transceiver model can be run for higher than 100 MHz and still gives a good performance, but the simulation time will be much longer. Actually this can be considered as one of the main drawbacks of using SIMULINK®, since it is relatively slow when running a model with either a very small time step or high frequency components.

9.3. FSK and Gaussian minimum shift keying (GMSK) comparison

In order to compare the developed FSK model performance with other modulation schemes, the Gaussian minimum shift keying (GMSK) was chosen for this purpose. GMSK is an attractive option for its excellent power and spectral efficiency. In Fig. 19, the BER of the FSK model with different frequency shifts is compared with that of a GMSK transceiver for a carrier frequency of 1 MHz.

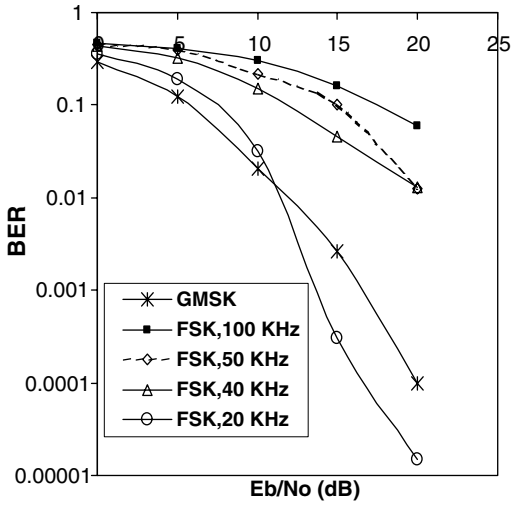

Fig. 19. Comparison of an FSK with different frequency shifts and a GMSK transceiver models.

It is clear that a frequency shift of 20 kHz is giving a comparable BER with a better performance for a higher SNR. This is due to the side lobes levels of the spectrum that are further reduced by reducing the FSK shifts.

9.4. Adjacent channel interference (ACI), inband/outband interference and multi-path effects

This is a phenomenon whereby channels that are beside one another in the frequency domain may have some spectral overlap, causing impairment and interference. The adjacent channel power ratio (ACPR) measures the amount of interference or power in an adjacent-frequency channel. Usually defined as the ratio of the average power in the adjacent frequency channel (or offset) to the average power in the transmitted-frequency channel. The ACPR describes the amount of distortion that is due to nonlinearities in the transmitter hardware. Fig. 20 clarifies the effect of ACI, where F_1 is the transmission frequency, f_{11} and f_{12} are the frequency components for both 0 and 1, respectively, and F_2 is an adjacent frequency channel. As shown in the figure, the two frequencies f_{12} and f_{21} are separated by a frequency guard band (GB).

The ACPR can be estimated by the following equation:

$$\mathrm{ACPR} = 10\log_{10}\left(\frac{V_2^2}{V_1^2}\right) = 20\log_{10}\left(\frac{V_2}{V_1^2}\right), \tag{16}$$

where V_1 and V_2 are the voltage signal levels of both the transmission and the adjacent channels. An investigation into the ACPR against the BER for different GB values is presented in Fig. 21 for the following parameters:

$F_1 = 1$ MHz,
frequency shift = 100 kHz,
output transmitter power = −85 dBm or −115 dB.

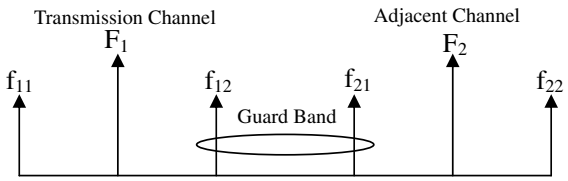

Fig. 20. Adjacent channel interference representation.

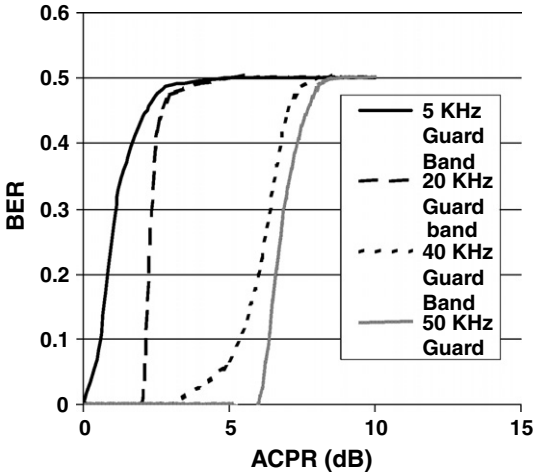

Fig. 21. Investigations the ACPR against BER for different guard band (GB) frequencies.

Fig. 22 clarifies the effect of the channel interference with different inband and outband signals assuming a noisy channel. Here, the transmission frequency is chosen to be 20 MHz with a channel bandwidth of 20 MHz. From the figure, the inner band interference (10–30 MHz) causes a high BER. The BER is significantly reduced below the edge of the lower outer band (nearly at 5 MHz). In the high outer band (30–40 MHz), the BER shows a similar behavior and then start to decrease.

In Fig. 23, the effect of the multi-path transmission is examined. It is clear that BER increases as the number of the paths that signal transmitted through increases.

9.5. Effect of channel encoding using error correcting codes (ECC)

Channel coding is used to correct the errors caused by noise during transmission. In this work, three different common ECC schemes have been introduced to investigate its impact on the overall system performance. These are [17]:

1. Binary Cyclic Codes BCC (15,5),
2. Bose–Chaudhuri–Hocquenghem codes BCH (15,5),
3. Hamming codes (15,11).

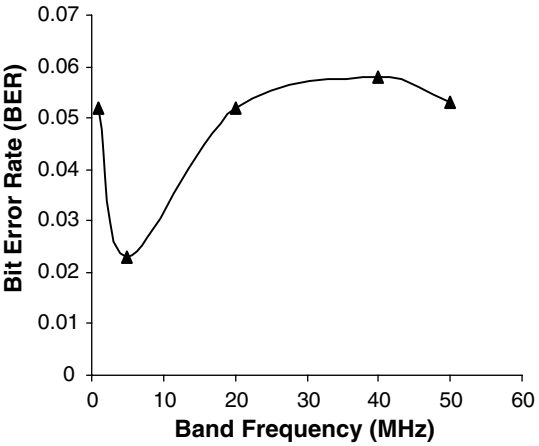

Fig. 22. BER performance in the presence of channel interference.

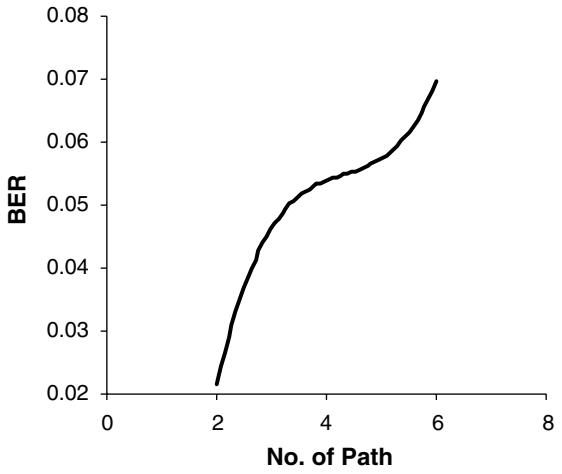

Fig. 23. Effect of the multi-path effect on the BER performance.

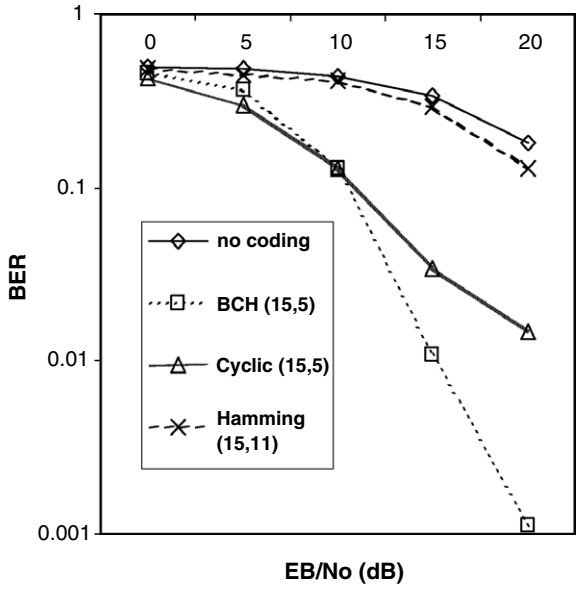

Fig. 24. BER performance against bit energy to noise power ratio (E_b/N_o) using UPCM with channel coding schemes.

The measured BER of the noisy RF channel using both NPCM and UPCM as a source encoding with three channel coding schemes are shown in Figs. 24 and 25.

From the two figures, it can be noticed that a good improvement in the BER is obtained when channel coding has been introduced. Obviously, the BCH scheme displays the best performance specially for high bit energy to noise power (E_b/N_o) ($\geqslant 10$ dB).

10. Testing compression

The performance of the compression implemented by the controller was assessed in terms of the total number of repeated and unrepeated frames that have to be sent to the receiver side. The three PCM methods were simulated initially at a rate of 1 kbps. The output rate of the controller after framing and multiplexing is 2.5 kbps. The results have been computed for both pH and pressure signals as shown in Tables 1 and 2 for total time of 50 s [18].

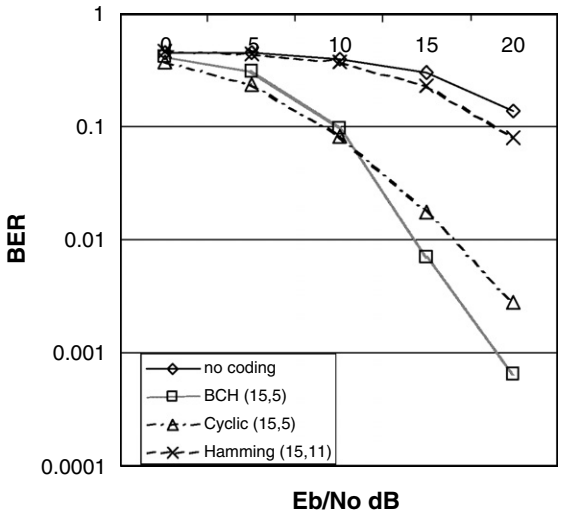

Fig. 25. BER performance against bit energy to noise power ratio (E_b/N_o) using NPCM with channel coding schemes.

In general, it is obvious from the tables that the number of the unrepeated frames for the pressure signal is more than that for the pH, since the pressure is changing rapidly. This means that the current sample of the pressure signal is most likely to be dissimilar from the previous one. In contrast to the pH signal in which, the current will stay the same to the previous for a longer time intervals.

A good ratio was obtained by using NPCM, where the signal was first compressed by the μ-function before a uniform encoding occurs, whereas DPCM has minimum compression ratio, since it is more sensitive to the differential change between the current and previous samples.

The distortion has been measured between the original and recovered waveforms for both pH and pressure as given in Table 3.

Table 1
Compression performance for pH signal

PCM coding algorithm (8 bits for sample)	pH frames sent	pH frames not sent	Compression ratio (%)
UPCM	437	4849	91.73
NPCM	662	4624	87.47
DPCM	2588	2698	51.04

Table 2
Compression performance for pressure signal

PCM coding algorithm (8 bits for sample)	PR frames sent	PR frames not sent	Compression ratio (%)
UPCM	3036	2250	42.56
NPCM	480	4806	90.10
DPCM	3321	1965	37.17

Table 3
Distortion measure of the system output signals using the PCM methods

PCM coding algorithm	pH signal distortion	Pressure signal distortion
UPCM	0.0104	0.0327
NPCM	0.8143	0.1309
DPCM	0.0284	0.1214

10.1. BER estimation with compression

The effect of the compression mechanism implemented on the performance of the channel BER was investigated [18]. Figs. 26 and 27 show the BER simulation results using both UPCM and NPCM, respectively. Basically the performance of the model has been improved for the two PCM methods by introducing the compression mechanism. The BER for the NPCM after 5 dB was greatly reduced by the compression. This is agreeing well with the results presented by Tables 1 and 2, as the amount of data compressed is much more less than for the other schemes. The same tests have been taken for the DPCM scheme as shown in Fig. 28.

It is clear from the graphs that a slight improvement in BER is obtained when the DPCM is working in the compression mode. This was expected as the amount of data compressed or stored and not sent are much less for the two schemes. As a result of this, the distortion caused by using the DPCM on the recovered signal at the receiver side is smaller compared with the NPCM. However, the UPCM proved to have a better performance in terms of the data compression and distortion effect.

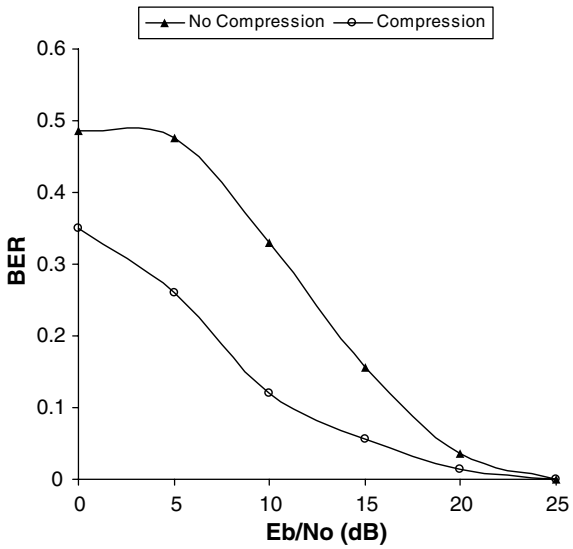

Fig. 26. Simulated BER performance against bit energy to noise power ratio (E_b/N_o) for FSK system using UPCM.

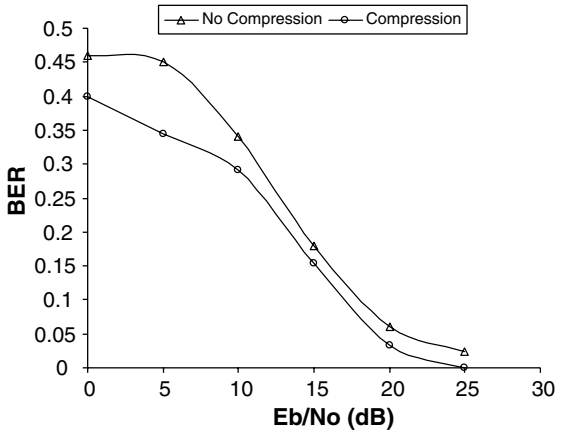

Fig. 27. Simulated BER performance against bit energy to noise power ratio (E_b/N_o) for FSK system using NPCM.

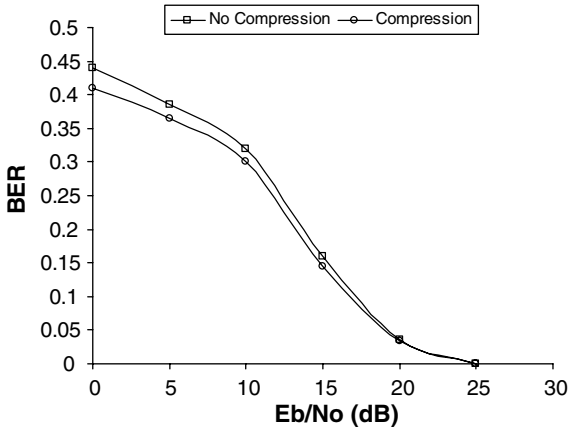

Fig. 28. Simulated BER performance against bit energy to noise power ratio (E_b/N_o) for FSK system using DPCM.

11. Testing decoder unit

In this unit, four reverse processes are performed to reconstruct the analog signals read by the pH and pressure sensors. These are De-multiplexing, De-framing, channel decoding, and source decoding. No need to mention that the performance of this unit is crucial to the system overall performance. The output signal-to-noise ration (SNR) of the output reconstructed analog data is used as an objective measure of the signal quality. Fig. 29 shows the output SNR against E_b/N_o using the three PCM source-encoding schemes for the pressure signal.

The improvement in the SNR using channel coding is also shown in Fig. 30, which presents the obtained SNR improvement using the three coding schemes for the pressure signal. As an initial conclusion, using UPCM as a source coding with BCH as a channel coding, a good performance was achieved.

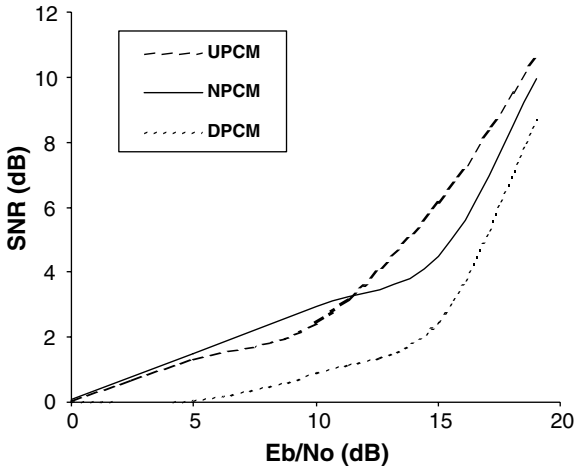

Fig. 29. Output SNR against bit energy to noise power ratio (E_b/N_o) using PCM source coding for pressure signal.

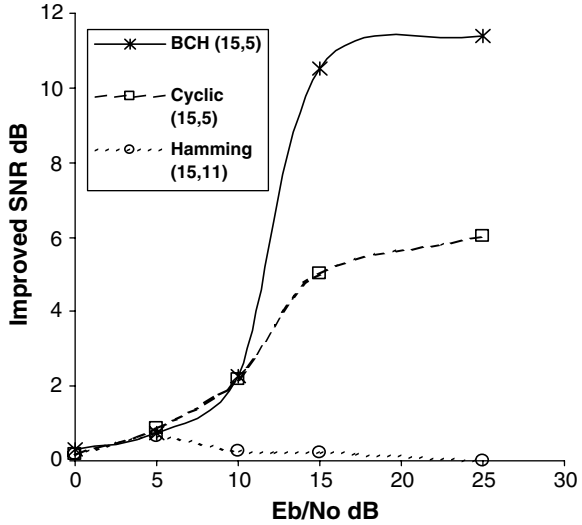

Fig. 30. Improved SNR against bit energy to noise power ratio (E_b/N_o) using the three channel coding schemes for pressure signal encoded with UPCM.

12. Conclusions

In this paper, a novel model for a wireless sensor data acquisition system based on PCM schemes has been presented. The system mainly consists of four main stages. The function of each stage was verified in relation to the other parts of the system. At the simulated controller unit, a compression mechanism based on sending only the unrepeated frames has been adopted.

Two types of real medical signals have been used to assess the model performance. An efficient FSK transmitter/receiver model has been simulated based on direct-conversion scheme.

It has been found that increasing the guard band frequency between the transmission and adjacent channels improves the BER performance of the system. At the same time increasing the ACPR leads to a sharp increase in the BER. The implemented model showed a good capability in recovering the original data at the receiver side with different transmission frequencies. From the presented results, a minimum distortion in the recovered signals in both, pH and pressure sensors were obtained by using the UPCM and DPCM. It was found that when the NPCM used in combination with the compression mechanism, a significant reduction in the amount of data transmitted through the channel is obtained. Finally, a good overall performance can be obtained by combining UPCM with BCH coding scheme.

It is necessary to mention that the transmission channel condition was the main effect considered in this study. As a future work, other effects like signal absorption caused by the human body biological tissues that have different dielectric properties and thicknesses will be introduced, although some amount of attenuation has been already added to the used medical signals.

Acknowledgments

This work was supported by the Enterprise Ireland Commercialization Fund 2003, under technology development phase, as part of the MIAPS project, reference no. CFTD/03/425. Funding was also received from the Irish Research Council for Science, Engineering and Technology: funded by the National Development Plan.

References

[1] T. Boon, E. Johannessen, L. Wang, A. Astaras, M. Ahmadian, A. Murray, J. Cooper, S. Beaumont, B. Flynn, D.R.S. Cumming, Toward miniature wireless integrated multisensor microsystem for industrial and biomedical applications, IEEE Sensors 1 (2002) 628–635.

[2] A. Mason, N. Yazdi, A. Chavan, K. Najafi, K.D. Wise, A generic multielement microsystem for portable wireless applications, IEEE Proc. 86 (1998) 1733–1746.
[3] T. Akin, K. Najafi, R.M. Bradley, A wireless implantable multichannel digital neural recording system for a micromachined sieve electrode, IEEE Solid State Circuit 33 (1998) 109–118.
[4] S. Chatzandroulis, D. Tsoukalas, A. Neukomm, A miniature pressure system with a capacitive sensor and a passive telemetry link for use in implantable applications, IEEE Microelectromechanical Syst. 9 (2000) 18–23.
[5] W. Claes, R. Puers, W. Sansen, De Cooman, J. Duyck, I. Naert, A low power miniaturized autonomous data logger for dental implants, Sensors Actuators 97–98 (2002) 548–556.
[6] L. Wang, T. Tang, E. Johannessen, A. Astaras, A. Murray, J. Cooper, S. Beaumont, D.R.S. Cumming, An integrated sensor microsystem for industrial and biomedical applications, in: Proc. of the IEEE Instrumentation and Measurement Technology Conference, Anchorage, USA, 2002, pp. 1717–1720.
[7] D. Kumar, S. Gustavsson, An Illustrated Guide to Gastrointestinal Motility, Wiley, London, 1988.
[8] W.C. Chu, Speech Coding Algorithms, Wiley, USA, 2003.
[9] A.M. Kondoz, Digital Speech, Wiley, Chichester, 1994.
[10] K. Arshak, E. Jafer, D. McDonagh, A. Arshak, D. Morris, O. Korostynska, D. Waldern, Modeling and simulation of a data acquisition system using PCM techniques, in: 3rd IEEE Conf. on Systems, Signals, and Devices, vol. IV, 2005.
[11] K. Kundert, Introduction to RF simulation and its application, IEEE Trans. Solid-State 34 (2001) 298–1320.
[12] B. Razavi, RF Microelectronics, Prentice-Hall PTR, NJ, USA, 1998.
[13] B. Razavi, Architectures and circuits for RF CMOS receivers, in: IEEE Custom Integrated Circuits Conference, 1998, pp. 393–400.
[14] W. Tranter, K. shanmugan, T.S. Rappaport, K. Kosbar, Principles of Communication Systems Simulation, Prentice-Hall PTR, NJ, USA, 2004.
[15] K. Arshak, E. Jafer, D. McDonagh, Simulation and testing of RF transceiver suitable for wireless short-range applications, in: IEEE Conf. Advances in Intelligent Systems – Theory and Applications, November 15–18, Luxembourg, 2004.
[16] J. Anderson, T.S. Rappaport, S. Yoshida, Propagation measurements and models for wireless communications channels, IEEE Trans. Commun. Mag. 33 (42–49) (1995).
[17] S. Lin, An Introduction to Error-Correcting Codes, Prentice-Hall, USA, 1970.
[18] K. Arshak, E. Jafer, D. McDonagh, Modeling and simulation of a wireless sensor data acquisition system using PCM algorithms, in: IEEE Behavioral Modeling and Simulation Conference, 21–22 October, San Jose, USA, 2004, pp. 80–85.